Hydrol. Earth Syst. Sci. Discuss., 11, 5037–5075, 2014
www.hydrol-earth-syst-sci-discuss.net/11/5037/2014/
doi:10.5194/hessd-11-5037-2014

Hydrology and Earth System Sciences
Open Access
Discussions

Evaluation of surface properties and atmospheric disturbances caused by post-dam alterations of land-use/land-cover

A. T. Woldemichael[1], **F. Hossain**[2], **and Sr R. Pielke**[3]

[1]Department of Civil and Environmental Engineering, Tennessee Technological University (Cookeville), Tennessee, USA
[2]Department of Civil and Environmental Engineering (Seattle) & QuESST (Tacoma), University of Washington, Washington, USA
[3]Senior Research Scientist, Cooperative Institute for Research in Environmental Sciences (CIRES), University of Colorado (Boulder), Colorado, USA

Received: 1 April 2014 – Accepted: 24 April 2014 – Published: 16 May 2014

Correspondence to: A. T. Woldemichael (abel_tad2000@yahoo.com)

Published by Copernicus Publications on behalf of the European Geosciences Union.

Abstract

This study adopted a differential land-use/land-cover (LULC) analysis to evaluate dam-triggered land–atmosphere interactions for a number of LULC scenarios. Two specific questions were addressed: (1) *can dam-triggered LULC heterogeneities modify surface and energy budget which, in turn, change regional convergence and precipitation patterns?* and (2) *how extensive is the modification in surface moisture and energy budget altered by dam-triggered LULC changes occurring in different climate and terrain features?* The Regional Atmospheric Modeling System (RAMS, version 6.0) was set up for two climatologically and topographically contrasting regions: the American River Watershed (ARW) located in California and the Owyhee River Watershed (ORW) located in eastern Oregon. For the selected atmospheric river precipitation event of 29 December 1996 to 3 January 1997, simulations of three pre-defined LULC scenarios are performed. The definition of the scenarios are: (1) the *control* scenario representing the contemporary land-use, (2) the *pre-dam* scenario representing the natural landscape before the construction of the dams and (3) the *non-irrigation* scenario representing the condition where previously irrigated landscape in the *control* is transformed to the nearby land-use type. Results indicated that the ARW energy and moisture fluxes were more extensively affected by dam-induced changes in LULC than the ORW. Both regions, however, displayed commonalities in the modification of land–atmosphere processes due to LULC changes, with the *control–non-irrigation* scenario creating more change than the *control–pre-dam* scenarios. These commonalities were: (1) the combination of a decrease in temperature (up to 0.15 °C) and an increase in dewpoint (up to 0.25 °C) was observed, (2) there was a larger fraction of energy partitioned to latent heat flux (up to 10 W m^{-2}) that increased the amount of water vapor to the atmosphere and resulted in a larger convective available potential energy (CAPE), (3) low level wind flow variation was found to be responsible for pressure gradients that affected localized circulations, moisture advection and convergence. At some locations, an increase in wind speed up to 1.6 m s^{-1} maximum was observed, (4) there

HESSD
11, 5037–5075, 2014

were also areas of well developed vertical motions responsible for moisture transport from the surface to higher altitudes that enhanced precipitation patterns in the study regions.

1 Introduction

LULC modifications, in the post-dam era, often lead to changes in land-surface (soil properties) and vegetation characteristics such as albedo, root distribution and roughness height (Beltran, 2005; Narisma and Pitman, 2003). For instance, Narisma and Pitman (2003) pointed out that conversion of a tree into grass reduces leaf area index (LAI), increases albedo and decreases roughness length. Zhao and Pitman (2002) found out that the change in vegetation cover from forest to grass and crops causes a large reduction in roughness height resulting in an increase in low-level wind fields. From a hydrometeorological point of view, such transformations affect the available water flow regime that influences soil moisture and precipitation. These changes also regulate the partitioning of energy between sensible and latent heat, boundary layer structures, local air temperature and wind patterns (Betts et al., 1996; Sud and Smith, 1985; Zhang et al., 1996; Zhao and Pitman, 2002).

Irrigation practices, which are one of the major post-dam LULC changes, for instance, can modify not only the precipitation pattern but also the surface moisture and energy distribution, which alter boundary layers and regional convergence, as well as mesoscale convection (Douglas et al., 2009). Irrigation has also an effect of cooling the ambient surface and near-surface temperature by decreasing the sensible heat fluxes and increasing latent heat fluxes (Boucher et al., 2004; Eungul et al., 2011), thus increasing the convective available potential energy (CAPE) (Pielke, 2001). The added moist enthalpy from irrigation tends to create strong spatial gradients of CAPE with respect to the surrounding non-irrigated landscape, which in turn can produce localized wind circulations. This process can enhance the likelihood of convective precipitation.

HESSD
11, 5037–5075, 2014

Another component of the post-dam induced LULC modification can be downstream urbanization. In urban landscapes, surface properties drastically are modified resulting in a modification of the energy budget and precipitation distribution (Shepherd, 2005). There is also an increase in surface roughness as compared to a previously uninhabited area. This increase in surface roughness creates a slower near-surface wind that facilitates convergence and assists in convective cell formation. Surface albedo also is modified as a result of the altered surface conditions due to urbanization.

It is plausible that the future points to a continuing trend for construction of more dams to satisfy societal demands for water and flood disaster alleviation, particularly in the developing world (Graf, 1999). As a result, LULC changes will also accelerate in the 21st-century (Pitman, 2003). The pressing issue, however, is how to create a scientifically credible link among the LULC changes that occur after the construction of a dam, the associated alteration in the land-surface properties and their interaction with atmospheric conditions.

The underlying objective of why the need arises to assess anthropogenic-land–atmosphere interactions should be perceived from the effect such assessments have on the formation and modification of precipitation. According to Georgescu (2008), the positive feedback created by the complex land–atmosphere interactions within the planetary boundary layer (PBL) establish a physical pathway for the enhancement of precipitation. Precipitation by itself can serve as a feedback mechanism (through the soil-precipitation feedback) by allowing for more soil moisture storage and further moisture supply through physical evaporation and transpiration, and precipitation recycling (Schar et al., 1998). Betts et al. (1996) also suggested that there is a positive feedback between soil moisture, surface evaporation and precipitation. This loop of complex interrelationship warrants the evaluation of all aspects of processes involved within the PBL in addition to precipitation.

In recent years, the scientific community has given attention to the impacts induced by LULC changes (such as irrigation and urbanization) on weather and climate. However, only a few quantitative and numerical modeling assessments address the effects

HESSD
11, 5037–5075, 2014

of the combined changes that are apparent due to the presence of dams (Hossain et al., 2012; Degu and Hossain, 2012; DeAngelis et al., 2010; Woldemichael et al., 2012, 2013) and contrasting settings. There remains a large gap in understanding the post-dam feedbacks due to LULC variability on surface properties and atmospheric disturbances.

Numerical modeling approaches, in a wide range of LULC scenarios, have been used to evaluate localized atmospheric disturbances. For instance, the regional atmospheric modeling system (RAMS) was applied for the assessment of interactions between atmospheric processes, such as mesoscale circulations and cloud formations, and land surface processes, such as heat and moisture fluxes from a set of different LULC scenarios (Stohlgren et al., 1998). The model was also implemented to evaluate the influence of anthropogenic landscape changes on the atmospheric conditions in South Florida (Pielke et al., 1999). The hydrometeorological effects of land-use heterogeneities on various spatial and temporal scales have also been modeled using different types of atmospheric models (Narisma and Pitman, 2006; Schneider et al., 2004; Marshall et al., 2010; Douglas et al., 2006; ter Maat et al., 2013).

This study focuses on the evaluation of human-land–atmosphere interactions, through a differential LULC change analysis, for a number of pre-defined LULC scenarios using the regional atmospheric modeling system (RAMS). The study tries to address the associated atmospheric disturbances due to variations in LULC properties that occur after dam construction for regions of different climatic zones. Moreover, the following two specific questions were addressed: (1) *can LULC heterogeneities that result due to the presence of a dam modify surface and energy budget which, in turn, change regional convergence and precipitation patterns?* and (2) *how extensive is the modification in surface moisture and energy budget altered by LULC changes near artificial reservoirs occurring in different climate and terrain features?*

Previous works reported in Woldemichael et al. (2012, 2013) investigated effects of land-use heterogeneities on modification of extreme precipitation for the same regions. Those studies reported that there was discernible alteration of extreme precipitation

HESSD
11, 5037–5075, 2014

that resulted from the dam-induced changes in LULC. Findings of the present study allow for comparisons of the role of the localized mesoscale circulations against the changes observed in the extreme precipitation patterns. The previous two works focused entirely on a numerical modeling approach to estimate extreme precipitation (EP) and discusses about how the engineering community can benefit from such approaches in a changing climate situations. In this paper, particular emphasis is made on the actual storm patterns which has very little to do with extremes. It is tried to addresses the behavior of storm dynamics and how this behavior is affected in a changing LULC situation.

As a broader impact, such findings can assist engineers and managers to establish weather and climate monitoring protocols, in addition to existing observation platforms, on regions where dam-induced LULC changes are prominent. The paper is organized as follows: Sect. 2 presents the study region. Section 3 explains the data and methods used in the study. Section 4 discusses the results. Finally, Sect. 5 presents the conclusions and recommendations of the study.

2 Study regions

Based on climatological and topographical contrasts, the Folsom dam and reservoir on the American River, windward of the Sierra-Nevada, and the Owyhee dam and reservoir on the Owyhee River, leeward of the Cascades, were selected for this study. The Folsom dam is located about 20 miles northeast of the city of Sacramento, California (Ferrari, 2005). The reservoir impounds the American River above Folsom dam that covers a watershed area of 4823 km^2 (US Army Corps of Engineers, USACE, 2005). The major purposes of the reservoir include irrigation, water supply, power generation, flood control and recreation. The climate of the American River watershed (ARW) is predominantly continental that receives rain primarily during the winter season (http://www.eoearth.org/article/).

HESSD
11, 5037–5075, 2014

The Owyhee dam, on the other hand, is located in Malheur County, Oregon and its reservoir impounds a watershed area of 26 617 km^2 (US Bureau of Reclamation, USBR, 2009). The major purpose of the reservoir is to irrigate the arid deserts occupied by the Owyhee irrigation district. Other purposes also include flood damage reduction, fishery, recreation and hydropower. The Owyhee River watershed (ORW) predominantly belongs to dry (arid) climate that receives little or no precipitation during most of the year.

The Folsom dam and the Owyhee dam became functional in 1955 and 1932, respectively. During the post-dam era, the natural landscape altered significantly in both regions where land was converted to irrigated agriculture and downstream regions became more urbanized. Figure 1 shows the contemporary LULC of both ARW and ORW along with the simulation domains as of 2003. The post-dam era had also experienced extreme flood events that resulted in unprecedented damage in life and property. For instance, both regions were highly affected by the 1996–1997 flood (the so-called the *new-year's* eve flood) where very heavy precipitation generated a devastating runoff that triggered a relook of management and operation of the dams.

The common underlying hydrometeorological factor that contributed to the 1996–1997 flooding episode was the presence of "Atmospheric Rivers" (AR's), which accounted for advective transport of water vapor along highly concentrated streamlines (Dettinger et al., 2012). The AR's that extended over much of California and the Pacific Northwest, when assisted with a strong low-level wind, carried large amount of moisture from the Pacific Ocean that eventually precipitated inland. In this study, we put forward the premise that dam-induced LULC changes during the post-dam era may have further influenced the storm through human-land–atmosphere feedback mechanisms. We hypothesize that these LULC changes played a role in modifying the surface properties and atmospheric circulations creating a path way for precipitation intensification for the 1996–1997 event. Accordingly, this study selected the 1996–1997 heavy precipitation episode. Moreover, the 1996–1997 flood episode is consistent with the flood period studied in previous separate works of extreme precipitation modification

HESSD
11, 5037–5075, 2014

on ARW and ORW (Woldemichael et al., 2012, 2013). Consistency in the study periods allowed us to explore a relationship among the observed extreme precipitation and the forcings and feedbacks for the precipitation formation. Moreover, the winters in these regions are favorable seasons for crops that cannot take the summer heat and hence the anticipated LULC change is also there in the winter time.

3 Data and methods

3.1 Land-use/land-cover (LULC) scenarios

Figure 1 shows the existing state of the LULC in the respective study regions as per the MODIS land cover type product (MCD12Q1, https://lpdaac.usgs.gov/). The MODIS-LULC, with a footprint of 500 m × 500 m, uses a supervised classification algorithm that is estimated by utilizing database of high quality land cover training sites developed using high resolution imagery (Muchoney et al., 1999).

The first LULC scenario, the *control* (as shown in Fig. 1 top panel), represents the contemporary landscape of the study regions. In order to separate out the influence of the irrigated agriculture on land–atmosphere interaction the second scenario represented the *non-irrigation*. Finally, the third scenario, the *pre-dam,* assimilated the no-dam/reservoir condition with the natural (undisturbed) landscape. These LULC scenarios are established based on the hypothesis that most anthropogenic changes around dams are prominent right after the dam becomes functional (i.e. the post-dam represented by the *control* scenario in this case).

In order to represent the *non-irrigation* scenario, irrigation extent was initially extracted from the global maps of irrigated areas from the Oak Ridge National Laboratory Distributed Active Archive Center (ORNL DAAC) for biogeochemical dynamics data source (also found at http://webmap.ornl.gov/). The initial extractions are shown in Fig. 2a and c both for ORW and ARW, respectively. The grid cell units are provided as percentage coverage and, in this study, regions with 50 % or more irrigation coverage

HESSD
11, 5037–5075, 2014

in each grid cell are predominantly assumed to be irrigated. This kind of approach has also been previously adopted in the works of Douglas et al. (2009), where they assumed a threshold of 50 % or more as irrigated cropland. Accordingly the irrigated patch was generated with this assumption and is shown as an overlay map (Fig. 2b and d). To represent the *non-irrigation* scenario, this land coverage is converted to the nearby land cover type (woody savanna in case of ARW and grassland in case of ORW). The urban area is also hypothetically assumed to be converted accordingly.

In order to represent the *pre-dam* scenario, there were a set of steps followed in the process of re-creating the 1950's LULC for ARW and the 1930's LULC for ORW, respectively. The transformations were made in closer proximity to the respective watersheds. First, the pre-dam land-use for both regions was extracted from the History Database of the Global Environment (HYDE) website (also available at http://themasites.pbl.nl/tridion/en/themasites/hyde/download/index-2.html). HYDE was developed under the authority of the Netherlands Environmental Assessment Agency and presents gridded time series of population and land-use for the last 12 000 years. According to HYDE, land-use was allocated as *cropland* and *grassland* under six assumptions mentioned on the HYDE site, and in this study, the 1950's land-use for ARW and the 1930's land-use for ORW were extracted. The percent coverage of each crop and grass is spatially represented in Fig. 3a and c for ORW and Fig. 4a and c for ARW. The analysis was made with the aid of the Geographical Information System (GIS).

Second, the representation of the cropland and grassland was made by considering which one of the two dominated in each grid cell (by considering the grid cells having more than 75 % of coverage to be representative). For instance, from Figs. 3c and 4c, the maximum percent coverage for grassland is 32 % for ORW and 36 % for ARW, respectively and it is assumed that 24 % or more (i.e. 75 % of the Maximum) for ORW and 27 % or more (i.e. 75 % of the maximum) for ARW are considered predominantly grasslands. These transformations are indicated by the green patches in Fig. 3d and the hatches in Fig. 4d. However, in case of the ORW, the grassland coverage that was predominant in the pre-dam persisted in the post-dam era (the 2003 LULC shown in

HESSD
11, 5037–5075, 2014

Fig. 3d), hence, no transformation was required for it. For cropland, 50 % in grid cell or more for both regions was considered as predominant (Figs. 3b and 4b). The pre-dam extents of the city of Sacramento downstream of Folsom dam and Boise City downstream of Owyhee dam are also included in the merged LULC representation.

Finally, merging procedure between the current land-use and the re-constructed croplands and grasslands as well as the urban regions was performed. The fact that there are only two broad classifications in the HYDE scheme (i.e. cropland and grassland), allows for the HYDE's $\sim 82\,km^2$ (9 km × 9 km) grid extent to be merged with the fine-tuned (current) LULC used for the analysis. Tables 1 and 2 represent percentage coverage of the LULC classes in each of the considered scenarios along with the vegetation parameters for each class.

3.2 Atmospheric model

For this study, we used the Regional Atmospheric Modeling System (RAMS-version 6.0). RAMS was developed to investigate cloud and land surface atmospheric phenomena and interactions, among other atmospheric weather features (Pielke et al., 1992; Tremback et al., 1985). RAMS is most often used as a limited area model, and many of its parameterizations have been formulated for high resolution mesoscale grids. The model has been extensively used to model detailed land-use descriptions and various land use scenarios and their interactions with the atmosphere (Pasqui et al., 2000; Douglas et al., 2009; Woldemichael et al., 2012, 2013).

The grid domains used for this study are shown in Fig. 1. In both regions, a nested grid configuration was adopted. In ARW, the coarser gird (Grid-1) consisted of 60 × 40 grid points at 10 km intervals and it covered much of the northern California, part of western Nevada and small portion of the eastern Pacific Ocean. The nested grid (Grid-2) had 62 × 62 grid points spaced at 3.3 km interval and covered all of the ARW. In ORW, the coarser grid (Grid-1) consisted of 66 × 66 grid points at 10 km grid intervals and covered portions of Oregon, Idaho, and Nevada. The nested grid (Grid-2) consisted of 86 × 86 grid points at 3 km grid intervals and falls over the ORW. In both regions, 30

HESSD
11, 5037–5075, 2014

vertical levels were assigned with a vertical grid spacing of 100 m at the ground. The grid stretch ratio used was 1.15 up to 1.5 km and kept constant from there on up to the model top. In both cases, a 20 s time step was set for the Grid-1 and a 5 s for Grid-2.

In order to represent the land–atmosphere interaction in the model, the recent version of the Land–Ecosystem–Atmosphere Feedback model (LEAF-3) was used (Walko and Tremback, 2005). Accordingly, 11 soil layers, 1 snow layer and 10 patches per grid cell for vegetation were assigned. The level-3 cloud microphysics scheme was adopted for this study (Meyers et al., 1997). Lateral boundary condition was represented by Klemp and Wilhelmson scheme (Klemp and Wilhelmson, 1978).

Through a set of ensemble experiments for both regions (not shown here), a combination of cumulus parameterization and radiative schemes that best represent an observed spatial precipitation pattern were selected. These results were independently reported in the works of Woldemichael et al. (2012) for ARW and Woldemichael et al. (2013) for ORW and the reader is encouraged to refer to those works. Accordingly, the short- and long-wave radiative transfer parameterization for both regions was furnished through the Harrington scheme (Harrington, 1997). The Kain–Fritsch (1993) convective parameterization was used for deep cumulus clouds in ORW, while the Kuo parameterization scheme was adopted for ARW (Kuo, 1974). The reason for using the relatively old Kuo parameterization for ARW was based on previous works of Castro (2005) which suggested that the Kain–Fritsch scheme generally overestimated precipitation in steep topography regions.

The inputs for RAMS model initialization were furnished by the National Center for Environmental Prediction/National Center for Atmospheric Research (NCEP/NCAR) reanalysis data (Kalnay et al., 1996). The surface characteristic datasets were obtained from the Atmospheric-Meteorological and Environmental Technologies (ATMET) data archive (available at http://www.atmet.com). These datasets include digital elevation model (DEM) data at 30 s (~ 1 km) spatial increments, soil moisture at various levels, the Normalized Difference Vegetation Index (NDVI), sea surface temperature (SST), and LULC.

HESSD
11, 5037–5075, 2014

4 Results and discussion

The surface and atmospheric analyses presented hereafter discusses the results obtained in the land–atmosphere interaction and related atmospheric dynamical processes. These analyses were done in the context of actual dam-induced LULC evolution that occurred in the study regions. They also discuss the link between surface energy budget changes with the mesoscale convection initiation and observed heavy storm system in the study period. Atmospheric fields were updated every 6 h interval based on the availability of the NCEP/NCAR reanalysis data. For the purpose of nudging the simulated values to the observed ones, and hence, remove any undesirable model drift, 4-dimenssional data assimilation (4DDA) was activated in the model. To analyze the impact of LULC changes related to the presence of dams, a selected six-day period (29 December 1996 to 3 January 1997) during the winter was primarily used. This period corresponds to an exceptional heavy rain episode over both regions which was responsible for causing devastating flooding and property damage. The accumulated 6 day precipitation amount for both regions is shown on Fig. 1 lower panel.

4.1 Surface analysis

The lowest model level (1000 mb) temperature averaged during the day over the heavy storm episode in ARW was seen to be lower (up to 0.15 °C) for most of the domain in the *control* (or with the current irrigation) case as compared to the *non-irrigation* case as shown in Fig. 5a. The decrease in the temperature corresponded to the regions where irrigation was intensified, indicating (expectedly) that irrigation had a tendency to suppress surface temperature and cause regional cooling. However, the pre-dam scenario showed little difference in temperature from the control as shown in Fig. 5c. In fact, the control was seen to be warmer than the pre-dam at the downstream of Folsom dam. This perhaps is due to the fact that much of the downstream area of Folsom was urbanized and the urban heat island effect was likely dominant, causing a much warmer surface environment than the pre-dam settlement. In case of ORW, although

HESSD
11, 5037–5075, 2014

both the *control–non-irrigation* and *control–pre-dam* differences were relatively small; the temperature was found to be lower and coincided with the region where irrigation had been introduced.

The dew point was seen to be higher in the *control* (up to 0.25 °C over the heavy storm episode period) than the *non-irrigation* as well as for the *pre-dam* as shown in Fig. 5b, d, f and h. The result clearly indicated that irrigated agriculture created higher dew-points provided that crops transpire and water applications were more frequent. This result also agrees with the findings of Mahmood et al. (2007) who evaluated dew-point temperature increases as a result of land use change. In areas where natural landscape was converted to irrigated agriculture, as already observed previously, the near surface air temperature was changed (Karl et al., 2012; Fall et al., 2010). These transformations have been seen to increase the dew point temperature as it was observed in California's central valley, which was converted from natural vegetation to agriculture (Sleeter, 2008).

It is understood that transformation of a non-irrigated region into irrigated agriculture results in partitioning of sensible heat and latent heat, and hence, affecting the surface energy balance (Mahmood et.al, 2007). It also results in reduction of mean daily temperature as shown in Fig. 5. An increase in soil moisture, as a result of irrigation, decreases the sensible heat while increasing the latent heat with respect to the *control* case. Figure 6a–h compared the energy fluxes for all the scenarios in ARW and ORW. The LULC transformation from the *pre-dam* to the *control* appeared to have a limited effect both on ARW and ORW as far as areal extent is concerned (Fig. 6b, d, f and h). In the inner grids of ARW sensible heat increased up to 21 $W m^{-2}$ and latent heat decreased on the order of more than 10 $W m^{-2}$.

The ARW region experienced a change of cropland into*irrigated* cropland (rain-fed) in the post-dam era. The albedo and the roughness height (Table 2) were similar for these two land-uses. Pitman (2003) pointed out that changes in roughness height play a prominent role in variations in sensible and latent heat fluxes. The majority of the land-use in ORW, on the other hand, remained the same (i.e. grassland: Fig. 3) for

HESSD
11, 5037–5075, 2014

most of the domain and as a result showed only a slight variability both in the sensible as well as latent heat. On the contrary, the change from *non-irrigation* to *control* has resulted in a larger spatial variability of the energy fluxes. In ARW, the exact location were the previously irrigated land was converted to nearest land-use pattern (i.e. woody savanna) in the *control–non-irrigation* case, showed a decrease in the sensible heat flux on the order of 15 $W m^{-2}$ or greater. An exception was the Sacramento urbanized region where the sensible heat flux was greater due to the UHI effect. Inversely, the latent heat increased up to 10 $W m^{-2}$ in the converted regions.

The combined comparison between sensible heat and the amount of latent heat is often essential in the energy balance determination. The comparison is usually made with the help of the Bowen ratio that represents the ratio between sensible and latent heat. In ORW region, due to its arid nature and that only small portion was under irrigation, the Bowen ratio was seen to be much higher as compared to the ARW, which had a more humid climate and where much of the downstream area was in active irrigation. Figure 7a–c and d–f presents the Bowen ratio for ARW and ORW. Comparison of the average Bowen ratio in each region revealed that it successively decreases from the *non-irrigation* to the *pre-dam* and to the *control* (Fig. 7a–c and d–f, respectively). This decrease was an indication that as the land gets more irrigated due to the presence of the dam, the sensible heat diminishes while all the available energy is converted into latent heat fluxes. A more significant transformation was observed in the change between the *non-irrigation* to *control* compared to the *pre-dam* to *control* results due to its less difference in land use change.

4.2 Atmospheric disturbance analysis

The partitioning of surface energy into sensible and latent heat has been a major driver of atmospheric circulations and convection in most parts of the world (Pielke, 2001). As established in the previous section, small thermal gradients across the landscape and lower atmosphere were created due to the surface energy budget variability. The low

HESSD
11, 5037–5075, 2014

level wind flow can also be affected as a result of the chain effects of LULC variability and resultants in creation of local horizontal pressure gradients.

In order to investigate the dam-induced anthropogenic changes on the wind flow, early afternoon conditions at ARW and ORW were considered. Figure 8a–d represents the averaged low level (1000 mb level) atmospheric wind speed and direction differences for both regions. Looking at the wind vectors closely, there were regions of convergence on the north-western end in ARW and northern end in ORW. In the ARW's *control–non-irrigation* scenario, the presence of irrigation has obviously increased the wind flow by an amount of 1.6 m s^{-1} or more in areas where land cover change was introduced. This is due to the fact that a land cover type characterized by larger roughness height (i.e. woody savanna with Z_o = 1.5 m, Table 2) in the *non-irrigation* case was converted into an irrigated cropland (Z_o = 0.06 m) in the *control* case. The difference in the roughness height (Z_o) had clearly contributed to locally induced wind flows in the region.

The *control–pre-dam* scenario of the ARW, however, showed a reduction in the wind speed (up to −1.4 m s^{-1} in magnitude) confined in a small area. The land-cover change in this case was characterized by the expansion of the city of Sacramento in the *control* case and the drag caused by buildings in cities was responsible in reducing the speed. In ORW, a small area convergence was observed in the inner grid north-eastern location. The control seemed to have lower magnitudes of wind speed (up to −0.4 m s^{-1} difference) from both the non-*irrigation* and *pre-dam*. The types of land-use transformations in both scenarios had a modest difference in roughness height than the control. In case of *non-irrigation*, the irrigated cropland was converted into grassland (roughness height, Z_o = 0.06 m and 0.04 m respectively, Table 1) while in the case of the *pre-dam* the predominant land-use type (i.e. grassland) remained unaltered for the majority of the area. However, the small area wind speed difference observed in *control–non-irrigation*, as explained above, could be due to the drag effect resulting from the expansion of the city.

HESSD
11, 5037–5075, 2014

Another analysis was performed at the mid-level of the maximum depth of the planetary boundary layer (PBL). The average depth of the RAMS generated PBL for each scenario as well as region is presented in Fig. 9. The mid-level PBL depth for ARW was at 1750 m above the ground while for ORW it was at 1000 m above the ground. The respective wind magnitudes and directions midway through the PBL are shown in Fig. 10a–d. At this level, the convergence zones in ARW tend to disappear unlike the wind directions noted on the low-level. On the other hand, the convergence zones, where two prevailing wind flows meet and interact, within ORW still existed midway through the PBL, which indicates a stronger mesoscale circulation. These observations indicated that, in case of ARW, the changes observed in the latent and sensible heat fluxes influence only the lower boundary layer wind flow. However, in both cases, local and mesoscale upward motion regions resulted from the low level convergence for both the ARW and ORW. This documents that the circulations due to LULC changes can transport moisture and heat higher into the atmosphere as discussed below:

The specific low level convergence location selected for analysis was at 39.3° N latitude for ARW and 43.4° N latitude for ORW. These locations were consistent with the region where cool and moist airs from the irrigated regions contrasted with relatively drier air from the nearby locations (indicated by the horizontal line in Fig. 8). Figure 11a–d shows the vertical cross section of simulated water vapor mixing ratio differences from the lowest level up to the top of the PBL (3500 m for ARW and 2000 m for ORW) for the six day averages of 22:00 UTC (or 14:00 LST). Figure 11a and b is for ARW: *control–non-irrigation* and *control–pre-dam* respectively. Both scenarios showed well developed vertical motion that was responsible in transporting moisture from the surface to higher altitudes. The same was true for the ORW (Fig. 11c and d). In this case the moisture was transported much deeper than the PBL indicating a much stronger vertical motion established in ORW than ARW. In both regions, the dense area of moisture transport corresponded to the location where wind convergence occurred.

Finally, to understand the availability of potential energy and convective contribution for precipitation formation, a Convective Available potential Energy (CAPE) analysis,

HESSD
11, 5037–5075, 2014

was performed. Figures 12 and 13 indicate the amounts of CAPE in the atmosphere for ARW and ORW respectively during the considered 6 days of analysis. Although the CAPE values were not large enough to warrant a convective initiation in the regions, there was a progressive increase in CAPE value from 29 December 1996 to 3 January 1997, mostly in the ARW. In all cases, the observed increase in CAPE originated from the increase in the latent heat flux in much of the northwest in ARW and eastern parts of ORW. There is also the important question as to how LULC affects these synoptically driven winter time systems. Since positive CAPE is recognized as a major factor that is altered by LULC, yet, during most days in the winter in the study regions, there is no CAPE, the general impression is that LULC effects on precipitation cannot work in these situations.

However, during these synoptically driven rain events, CAPE is often quite positive. Severe thunderstorms (with documented strong convective instability) and even tornadoes occur during these events (e.g. Hanstrum et al., 2002; Kingsmill et al., 2006) (see also https://ams.confex.com/ams/pdfpapers/115125.pdf). Our results indicated that during these precipitation events, a significant fraction involves deep cumulus clouds, and thus changes in CAPE, and other thermodynamic aspects of the atmosphere by LULC result in alterations in precipitation from what otherwise would have occurred.

5 Summary and conclusions

Precipitation is highly dependent on both the vertical and horizontal pathways of water vapor flux. How dam-induced mesoscale atmospheric changes in an impounded region impact these fluxes needs to be further understood. In this study, a number of more primitive variables that accompany heavy precipitation patterns were evaluated. The Regional Atmospheric Modeling System (RAMS) was set up to model two impounded regions with climatic and topographic contrasts: the Folsom dam in American River Watershed (ARW) and the Owyhee dam in Owyhee River Watershed (ORW). For each

HESSD
11, 5037–5075, 2014

of these regions, three experimental LULC scenarios were established: (1) the *control* scenario representing the contemporary land-use, (2) the *pre-dam* scenario representing the natural landscape before the construction of the dams and (3) the *non-irrigation* scenario representing the condition where previously irrigated landscape in the *control* is transformed to the nearby land-use type. Based on these scenarios, a differential LULC (i.e. *control–non-irrigation* and *control–pre-dam*) evaluation was performed to evaluate surface energy changes and atmospheric disturbances.

From the point of view of locations, the ARW was found to be more sensitive to associated changes in energy and moisture fluxes than the ORW. This perhaps is due to the fact that the areal extent of LULC change in the ARW is much greater than that of the ORW. It was also reported in our previous work (Woldemichael et al., 2013) that the post-dam LULC change scenarios impact precipitation of ORW (Owyhee Dam) much more than that of the ARW (Folsom Dam). We hypothesized that, due to its semi-arid climate and flat terrain, the ORW was very sensitive to even slight changes in the variables that lead to precipitation modification than for the ARW, which is in a humid climate and mountainous terrain (Jeton et al., 1996; Vaccaro, 2002).

However, both regions showed a strong link between the sensitivity of the surface energy and moisture fluxes and precipitation in the LULC assessment. More prominently, the *control–non-irrigation* cases showed a much higher impact than the *control–pre-dam* conditions, which perhaps is because of larger roughness height (Z_o) differences in the former case. Similarly, previous work indicated that precipitation modification was found to be much higher in the *control–non-irrigation* cases in ARW as well as ORW (Woldemichael et al., 2012). Both regions, however, displayed atmospheric conditions for a significant modification in precipitation to occur: (1) the combination of a decrease in temperature (up to 0.15 °C and an increase in dewpoint (up to 0.25 °C) was observed, (2) similar to the finds of Douglas et al. (2009), there is a larger fraction of energy partitioned to latent heat flux (up to 10 $W m^{-2}$) that increases the amount of water vapor flux into the atmosphere and result in a larger convective available potential energy (CAPE), (3) low level wind flow variation was found to be responsible in

HESSD
11, 5037–5075, 2014

creating a pressure gradient that affects localized circulations and moisture advection and convergence. An increase in wind speed up to 1.6 $m s^{-1}$ maximum was simulated in the regions due to the chain effects of LULC variability, (4) there were well developed vertical motions that can transport moisture from the surface to higher altitudes, and these were observed at locations where the precipitation difference was also a maximum. All of these findings further reinforced the fact that there is a strong correlation between the changes in surface and atmospheric properties, and corresponding resultant precipitation modification.

The 2003 Climate Change Science Program (CCSP 2003) proposed assessment strategies to understand how current and predicted changes in LULC will modify weather and climate. The report specifically mentioned that "*assessment capabilities should include the means to evaluate the interactions of land use and management with climate change in a way that will help decision makers mitigate or adapt to the change.*" It was also mentioned that both climate systems and anthropogenic activities that result in LULC changes are complex processes. In this regard, this study has shed light on two important aspects: (1) the LULC alterations that result from dam construction, which is a new paradigm in the process of human-induced LULC change assessment, and (2) the distinctiveness of land–atmosphere interaction of dam-driven LULC changes as a function of location.

Acknowledgements. The first author was supported by a NASA Earth System Science (NESSF) fellowship grant (NNX12AN34H). The authors acknowledge the technical support received from Mike Renfro of the Computer-Aided Laboratory at the Center for Manufacturing Research, Tennessee Technological University, who helped in the efficient set up of the RAMS model on various computing clusters. R. A. Pielke Sr. received support through the Vice Chancellor for Research at the University of Colorado in Boulder (CIRES/ATOC) and from NSF Grant AGS-1219833.

HESSD
11, 5037–5075, 2014

References

Betts, A. K., Ball, J. H., Beljaars, A. C. M., Miller, M. J., and Viterbo, P. A.: The land surface–atmosphere interaction: a review based on observational and global modeling perspectives, J. Geophys. Res., 101, 7209–7225, 1996.

Boucher, O., Myhre, G., and Myhre, A.: Direct human influence of irrigation on atmospheric water vapor and climate, Clim. Dynam., 22, 597–603, doi:10.1007/s00382-004-0402-4, 2004.

Castro, C. L.: Investigation of the summer climate of North America: a regional atmospheric modeling study, Ph.D. dissertation, Colo. State Univ., Fort Collins, 2005.

Climate Change Science Program: Strategic plan for the US climate change science program: Washington, D. C., 202 pp., available at: http://purl.access.gpo.gov/GPO/LPS64573, 2003.

DeAngelis, A., Dominguez, F., Fan, Y., Robock, A., Kustu, M. D., and Robinson, D.: Evidence of enhanced precipitation due to irrigation over the Great Plains of the United States, J. Geophys. Res., 115, D15115, doi:10.1029/2010JD013892, 2010.

Degu, A. M. and Hossain, F.: Investigating the mesoscale impact of artificial reservoirs on frequency of rain during growing season, Water Resour. Res., 48, W05510, doi:10.1029/2011WR010966, 2012.

Dettinger, M. D., Ralph, F. M., Hughes, M., Neiman, T. D. P., Cox, D., Estes, G., Reynolds, D., Hartman, R., Cayan, D., and Jones, L.: Design of quantification of an extreme winter storm scenarios for emergency preparedness and planning exercise in California, Nat. Hazards, 60, 1085–1111, doi:10.1007/s11069-011-9894-5, 2012.

Douglas, E. M., Niyogi, D., Frolking, S., Yeluripati, J. B., Pielke Sr., R. A., Niyogi, N., Vörösmarty, C. J., and Mohanty, U. C.: Changes in moisture and energy fluxes due to agricultural land use and irrigation in the Indian Monsoon Belt, Geophys. Res. Lett., 33, L14403, doi:10.1029/2006GL026550, 2006.

Douglas, E. M., Beltran, A., Niyogi, D., Pielke Sr., R. A., and Vorosmarty, C. J.: The impact of agricultural intensification and irrigation on land atmosphere interactions and Indian monsoon precipitation – a mesoscale modeling perspective, Global Planet. Change, GLOBAL-01425, 1–12, doi:10.1016/j.gloplacha.2008.12.007, 2009.

Eungul, L., Sacks, W. J., Chase, T. N., and Foley, J. A.: Simulated impacts of irrigation on the atmospheric circulation over Asia, J. Geophys. Res., 116, D08114, doi:10.1029/2010JD014740, 2011.

HESSD
11, 5037–5075, 2014

Fall, S., Deffenbaugh, N. S., Niyogi, D., Pielke Sr., R. A., and Rochon, G.: Temperature and equivalent temperature over the United States (1979–2005), Int. J. Climatol., 30, 2045–2054 doi:10.1002/joc.2094, 2010.

Ferrari, R. L.: Folsom Lake: 2005 sedimentation survey, report, Bureau of Reclam, Tech. Serv. Cent., Denver, Colo., 2005.

Georgescu, M.: Evaluating the effect of land-use and land-cover change on climate in the greater Phoenix, AZ, region, Ph.D. dissertation, Department of Atmospheric Science, the State University of New Jersey, 185 pp., 2008.

Graf, W. L.: Dam nation: a geographic census of American dams and their large-scale hydrologic impacts, Water Resour. Res., 35, 1305–1311, doi:10.1029/1999WR900016, 1999.

Hanstrum, B. N., Mills, G. A., Watson, A., Monteverdi, J. P., and Doswell, C. A.: The cool-season tornadoes of California and Southern Australia, Weather Forecast., 17, 705–722, doi:10.1175/1520-0434(2002)017<0705:TCSTOC>2.0.CO;2, 2002.

Harrington, J. Y.: The effects of radiative and microphysical processes on simulated warm and transition season Arctic stratus, Ph.D. dissertation, 289 pp., Colo. State Univ., Fort Collins, 1997.

Hossain, F., Degu, A. M., Yigzaw, W., Niyogi, D., Burian, S., Shepherd, J. M., and Pielke Sr., R. A.: Climate feedback-based considerations to dam design, operations and water management in the 21st century, J. Hydrol. Eng., 17, 837–850, doi:10.1061/(ASCE)HE.1943-5584.0000541, 2012.

Jeton, A. E., Dettinger, M. D., and Smith, J. L.: Potential Effects of climate change on Stream flow, Eastern and Western Slopes of the Sierra Nevada, California and Nevada, USGS, Water Resources Investigations Report 95–4260, 44 pp., 1996.

Kain, J. S. and Fritsch, M.: Convective parameterization for mesoscale models: The Kain-Fritsch scheme. The Representation of Cumulus Convection in Numerical Models, Meteorol. Mon., 24, American Meteorological Society, Boston, 165–170, 1993.

Kalnay, E.: The NCEP/NCAR 40-year reanalysis project, B. Am. Meteorol. Soc., 77, 437–471, doi:10.1175/1520-0477(1996)077<0437:TNYRP>2.0.CO;2, 1996.

Karl, T. R., Gleason, B. E., Menne, M. J., McMahon, J. R., Heim, J. R. R., Brewer, M. J., Kunkel, K. E., Arndt, D. S., Privette, J. L., Bates, J. J., Groisman, P. Y., and Easterling, D. R.: US temperature and drought: anomalies of spring and summer 2011-12 and trends, Eos Trans. AGU, 93, 473, 2012.

HESSD
11, 5037–5075, 2014

Kingsmill, D. E., Neiman, P. J., Ralph, F. M., and White, A. B.: Synoptic and topographic variability of northern California precipitation characteristics in landfalling winter storms observed during CALJET, Mon. Weather Rev., 134, 2072–2094, doi:10.1175/MWR3166.1, 2006.

Klemp, J. B. and Wilhelmson, R. B.: The simulation of three-dimensional convective storm dynamics, J. Atmos. Sci., 35, 1070–1096, 1978.

Kuo, H. L.: Further studies of the parameterization of the influence of cumulus convection on large-scale flow, J. Atmos. Sci., 31, 1232–1240, doi:10.1175/1520-0469(1974)031<1232:FSOTPO>2.0.CO;2, 1974.

Mahmood, R., Hubbard, K. G., Leeper, R. D., and Foster, S. A.: Increase in near-surface atmospheric moisture content due to land use changes: evidence from the observed dew point temperature data, Mon. Weather Rev., 136, 1554–1561, doi:10.1175/2007MWR2040.1, 2007.

Marshall Jr., C. H., Pielke Sr., R. A., Steyaert, L. T., and Willard, D. A.: The impact of anthropogenic land-cover change on the Florida peninsula sea breezes and warm season sensible weather, Mon. Weather Rev., 132, 28–52, 2010.

Meyers, M. P., Walko, R. L., Harrington, J. Y., and Cotton, W. R.: New RAMS cloud microphysics parameterization. Part II: The two moment scheme, Atmos. Res., 45, 3–39, 1997.

Muchoney, D., Strahler, A., Hodges, J., and LoCastro, J.: The IGBP DISCover confidence sites and the system for terrestrial ecosystem parameterization: tools for validating global land cover data, Photogramm. Eng. Rem. S., 65, 1061–1067, 1999.

Narisma, G. T. and Pitman, A. J.: The impact of 200 years of land covers change on the Australian near-surface climate, J. Hydrometeorol., 4, 424–436, 2003.

Narisma, G. T. and Pitman, A. J.: Exploring the sensitivity of the Australian climate to regional land-cover-change scenarios under increasing CO_2 concentrations and warmer temperature, Earth Interact., 10, 1–27, doi:10.1175/EI154.1, 2006.

Pasqui, M., Gozzini, B., Grifoni, D., Meneguzzo, F., Messeri, G., Pieri, M., Rossi, M., and Zipoli, G.: Performances of the operational RAMS in a Mediterranean region as regard to quantitative precipitation forecasts. Sensitivity of precipitation and wind forecasts to the representation of land cover, applied meteorology foundation, FMA, available at: http://www.atmet.com/html/workshop/workshop-4.shtml#43 (last access: 2 August 2013), 2000.

Pielke Sr., R. A.: A comprehensive meteorological modeling system – RAMS, Meteorol. Atmos. Phys., 49, 69–91, doi:10.1007/BF01025401, 1992.

HESSD
11, 5037–5075, 2014

Pielke Sr., R. A.: Influence of the spatial distribution of vegetation and soils on the prediction of cumulus convective rainfall, Rev. Geophys., 39, 151–177, 2001.
Pielke Sr., R. A., Walko, R. L., Steyaert, L. T., Vidale, P. L., Liston, G. E., Lyons, W. A., and Chase, T. N.: The influence of anthropogenic landscape changes on weather in south Florida, Mon. Weather Rev., 127, 1663–1673, doi:10.1175/1520-0493(1999)127<1663:TIOALC>2.0.CO;2, 1999.
Pielke Sr., R. A., Pitman, A., Niyogi, D., Mahmood, R., McAlpine, C., Hossain, F., Goldewijk, K., Nair, U., Betts, R., Fall, S., Reichstein, M., Kabat, P., and de Noblet-Ducoudré, N.: Land use/land cover changes and climate: modeling analysis and observational evidence, WIREs Clim. Change 2011, 2, 828–850, doi:10.1002/wcc.144, 2011.
Pitman, A. J.: The evolution of, and revolution in, land surface schemes designed for climate models, Int. J. Climatol., 23, 479–510, 2003.
Schar, C., Luthi, D., Beyerle, U., and Heise, E.: The soil feedback: a process study with a regional climate model, J. Climatol., 12, 722–742, 1998.
Schneider, N., Eugster, W., and Schichler, B.: The impact of historical land-use changes on the near-surface atmospheric conditions on the Swiss Plateau, Earth Interact., 8, 1–27, doi:10.1175/1087-3562(2004)008<0001:TIOHLC>2.0.CO;2, 2004.
Shepherd, J. M.: A review of current investigations of urban-induced rainfall and recommendations for the future, Earth Interact., 9, 1–27, doi:10.1175/EI156.1, 2005.
Sleeter, B. M.: Late 20th century land change in the Central California Valley Ecoregion, The California Geographer, 48, 27–60, 2008.
Stohlgren, T. J., Thomas, N. C., Pielke Sr., R. A., Kittles, T. G. F., and Baron, J. S.: Evidence that local land use practices influence regional climate, vegetation, and stream flow patterns in adjacent natural areas, Global Change Biol., 4, 495–504, doi:10.1046/j.1365-2486.1998.t01-1-00182.x, 1998.
Sud, Y. C. and Smith, W. E.: The influence of surface roughness of deserts on the July circulation – a numerical study, Bound.-Lay. Meteorol., 33, 15–49, 1985.
ter Maat, H. W., Moors, E. J., Hutjes, R. W. A., Holtslag, A. A. M., and Dolman, A. J.: Exploring the impact of land cover and topography on rainfall maxima in the Netherlands, J. Hydrometeorol., 14, 524–542, doi:10.1175/JHM-D-12-036.1, 2013.
Tremback, C. J., Tripoli, G. J., and Cotton, W. R.: A regional scale atmospheric numerical model including explicit moist physics and a hydrostatic time-split scheme paper presented at 7th

HESSD
11, 5037–5075, 2014

Conference on Numerical Weather prediction, Am. Meteorol. Soc., Montreal, Que., Canada, 433–434, 17–20 June, 1985.
US Bureau of Reclamation, USBR: The story of Owyhee Project, available at: http://www.usbr.gov/pn (last access: 19 May 2011), 2009.
US Army Corps of Engineers (USACE): Stochastic modeling of extreme floods on the American River at Folsom dam – flood frequency curve extension, Hydrol. Eng. Cent., Sacramento, Calif., 2005.
Vaccaro, J. J.: Interdecadal changes in the hydrometeorological regime of the Pacific Northwest and in the regional-to-hemispheric climate regimes, and their linkages, US Geological Survey, water resources investigation report, available at: http://pubs.usgs.gov/wri/wri024176/pdf/wri024176.pdf (last access: 21 June 2011), 2002.
Walko, R. L. and Tremback, C. J.: RAMS: Regional Atmospheric Modeling System, version 4.3/4.4 – Introduction to RAMS 4.3/4.4. ASTER Div., Mission Res., Inc., Fort Collins, Colo., 2002.
Woldemichael, A. T., Hossain, F., Pielke Sr., R. A., and Beltrán A.: Understanding the impact of dam-triggered land use/land cover change on the modification of extreme precipitation, Water Resour. Res., 48, W09547, doi:10.1029/2011WR011684, 2012.
Woldemichael, A. T., Hossain, F., and Pielke Sr., R. A.: Impacts of post-dam land-use/land-cover changes on modification of extreme precipitation in contrasting hydro-climate and terrain features, J. Hydrometeorol., 15, 777–800, doi:10.1175/JHM-D-13-085.1, 2013.
Zhao, M. and Pitman, A. J.: The impact of land cover change and increasing carbon dioxide on the extreme and frequency of maximum temperature and convective precipitation, Geophys. Res. Lett., 29, 1078, doi:10.1029/2001GL013476, 2002.

HESSD
11, 5037–5075, 2014

Table 1. ORW: – Percentage coverage of the LULC classes in each of the considered scenarios and vegetation parameters for each LULC class. (Source: Walko and Tremback, 2005: Modification for the Transition from LEAF-2 to LEAF-3, ATMET technical note.)

LULC-Class Name	Percent Area (%)			Albedo	Emissivity	Roughness height, Z_o (m)
	Pre-dam	Control	Non-Irrigation			
Urban and built up	0.50	0.80	0.40	0.15	0.90	0.80
Evergreen needleleaf forest	32.70	32.70	32.70	0.10	0.97	1.00
Deciduous needleleaf forest	1.70	1.70	1.70	0.10	0.95	1.00
Deciduous broadleaf forest	0.00	0.00	0.00	0.20	0.95	0.80
Evergreen broadleaf forest	0.00	0.00	0.00	0.15	0.95	2.00
Closed shrubs	2.70	2.70	2.70	0.10	0.97	0.14
Water	0.50	0.60	0.50	0.14	0.99	0.00
Mixed forest	0.60	0.60	0.60	0.14	0.95	0.40
Irrigated croplands	13.20	14.7	10.0	0.18	0.95	0.06
Grasslands	15.90	15.70	20.0	0.11	0.96	0.04
Savannas	1.00	1.00	1.00	0.20	0.92	1.50
Barren or sparsely vegetated	2.80	2.80	2.80	0.25	0.85	1.00
Woody savannas	16.10	16.10	16.10	0.20	0.92	1.50
Open shrublands	10.50	10.60	10.50	0.12	0.97	0.08
Crops, grass and shrubs	0.50	0.80	0.40	0.25	0.92	0.14

HESSD
11, 5037–5075, 2014

Table 2. ARW: – Percentage coverage of the LULC classes in each of the considered scenarios and vegetation parameters for each LULC class. (Source: Walko and Tremback, 2005: Modification for the Transition from LEAF-2 to LEAF-3, ATMET technical note.)

LULC-Class Name	Percent Area (%)			Albedo	Emissivity	Roughness height, Z_o (m)
	Pre-dam	Control	Non-Irrigation			
Urban and built up	1.18	3.83	3.73	0.15	0.90	0.80
Evergreen needleleaf forest	26.75	27.69	27.44	0.10	0.97	1.00
Deciduous needleleaf forest	0.79	0.84	0.81	0.10	0.95	1.00
Deciduous broadleaf forest	0.002	0.002	0.002	0.20	0.95	0.80
Evergreen broadleaf forest	0.002	0.002	0.002	0.15	0.95	2.00
Closed shrubs	0.27	0.892	0.71	0.10	0.97	0.14
Water	0.26	1.79	1.69	0.14	0.99	0.00
Mixed forest	1.43	0.81	0.77	0.14	0.95	0.40
Irrigated croplands	0.68	21.42	2.77	0.18	0.95	0.06
Grasslands	25.16	8.23	7.34	0.11	0.96	0.04
Savannas	2.56	1.91	1.73	0.20	0.92	1.50
Barren or sparsely vegetated	0.33	0.06	0.04	0.25	0.85	1.00
Woody savannas	17.94	31.80	52.28	0.20	0.92	1.50
Open shrublands	0.65	0.68	0.67	0.12	0.97	0.08
Crops, grass and shrubs	22.12	–	0.001	0.25	0.92	0.14

HESSD
11, 5037–5075, 2014

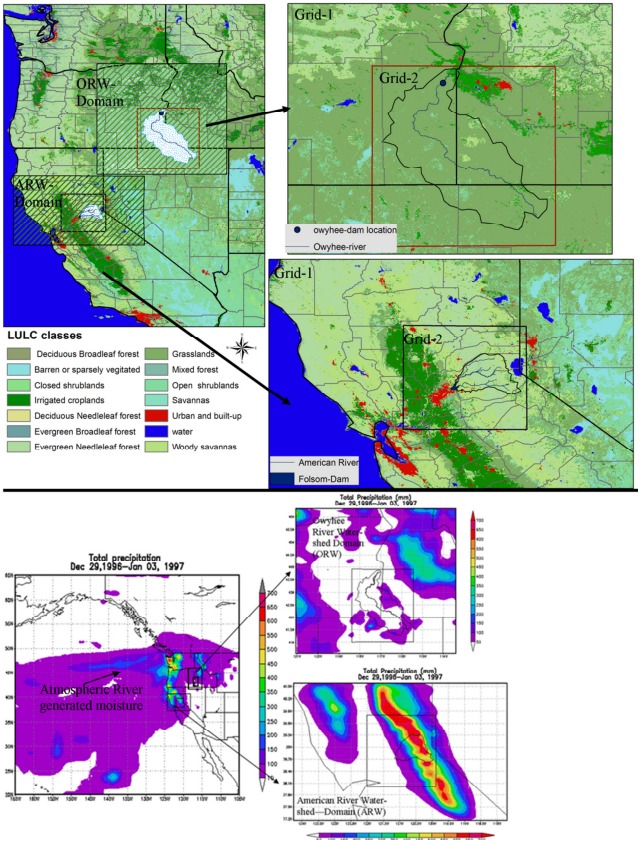

Fig. 1. The contemporary LULC (*i.e. Control* scenario) of the study regions along with simulation domains for both ARW and ORW (top panel). Courtesy of MODIS land cover type product or MCD12Q1 (also available at http://glcf.umiacs.umd.edu/). Lower panel represents 6 day total precipitation (maximum of 350 mm for ORW and 700 mm for ARW) that was result of the same Atmospheric River (AR) event.

HESSD
11, 5037–5075, 2014

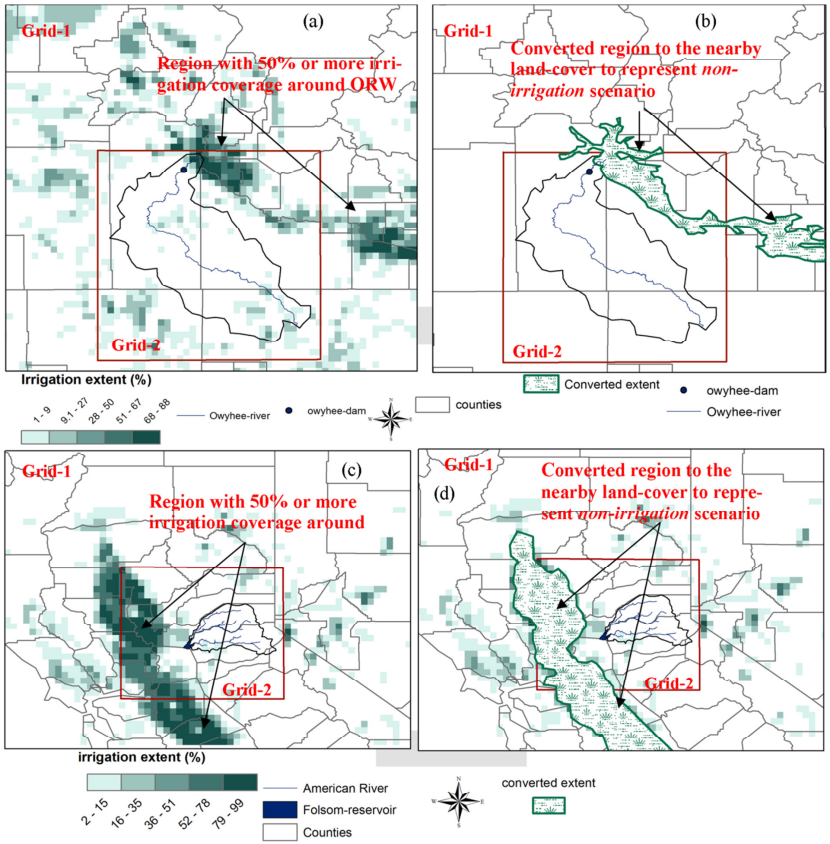

Fig. 2. Generated irrigated land cover to establish the *non-irrigation* scenarios. Irrigation extent initially extracted from the global maps of irrigated areas from the Oak Ridge National Laboratory Distributed Active Archive Center (ORNL DAAC) for biogeochemical dynamics data source (also found at http://webmap.ornl.gov/).

HESSD
11, 5037–5075, 2014

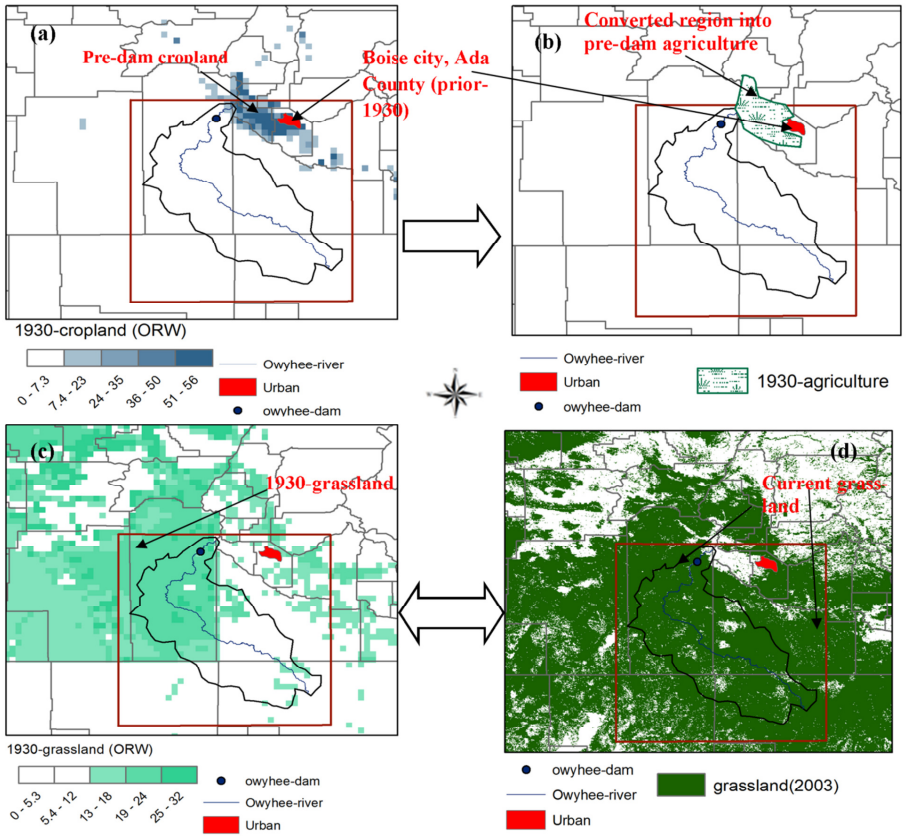

Fig. 3. Percentage (%) coverage of cropland and grassland over ORW (**a** and **c**), and derived croplands and grasslands for the 1930 pre-dam LULC analysis (**b** and **d**). courtesy of the History Database of the Global Environment (HYDE) website (also available at http://themasites.pbl.nl).

HESSD
11, 5037–5075, 2014

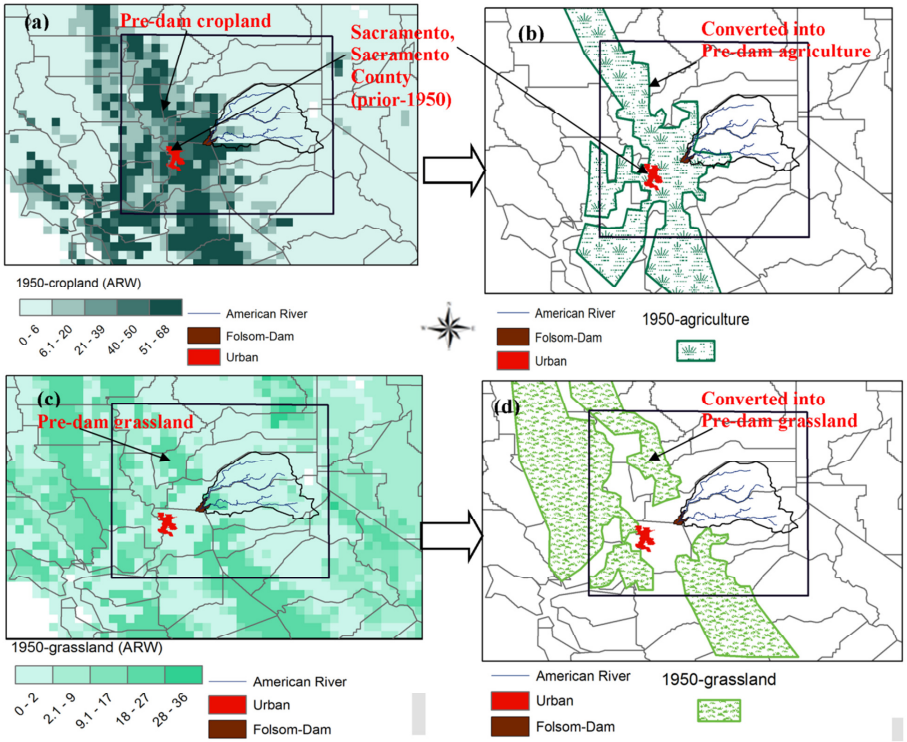

Fig. 4. Percentage (%) coverage of cropland and grassland over ARW (**a** and **c**), and derived croplands and grasslands for the 1950 pre-dam LULC analysis (**b** and **d**). Courtesy of the History Database of the Global Environment (HYDE) website (also available at http://themasites.pbl.nl).

HESSD
11, 5037–5075, 2014

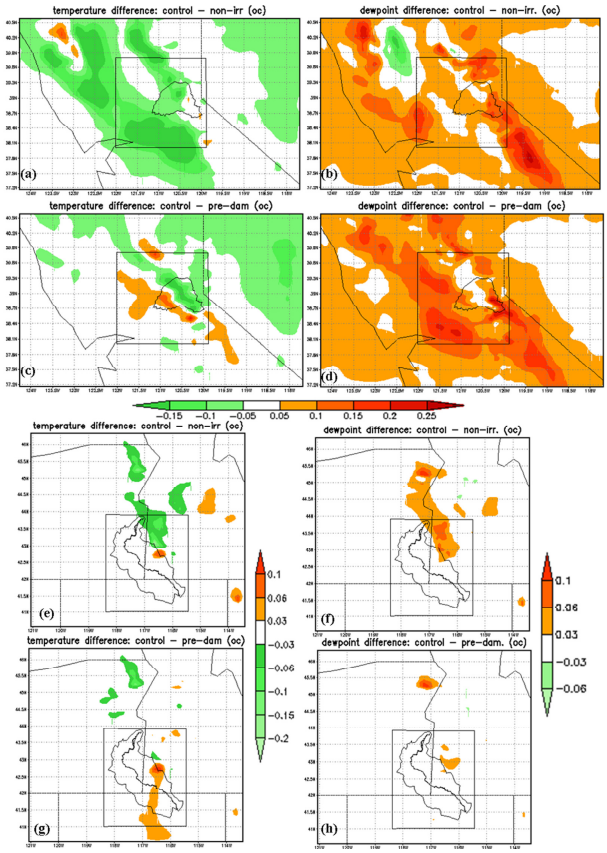

Fig. 5. Differences in surface temperature (˚C): (**a** and **e**) for *control–non-irrigation* for ARW and ORW, respectively. (**c** and **g**) for *control–pre-dam* for ARW and ORW, respectively. Differences in dew point temperature (˚C): (**b** and **f**) for *control–non-irrigation* for ARW and ORW, respectively. (**d** and **h**) for *control–pre-dam* for ARW and ORW, respectively.

HESSD
11, 5037–5075, 2014

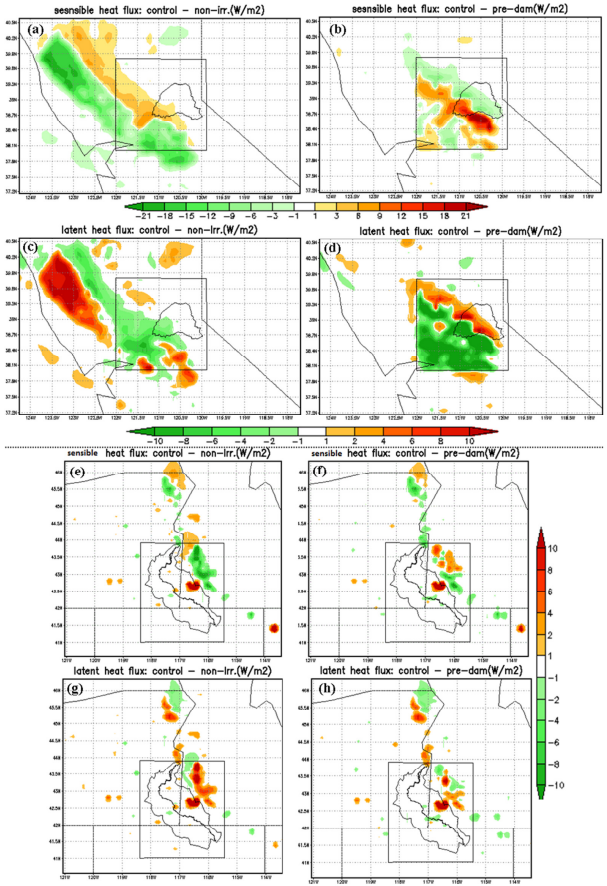

Fig. 6. Differences in sensible and latent heat fluxes ($W m^{-2}$). **(a)**, **(b)**, (**e** and **f**) differences for ARW and ORW, sensible heat fluxes, respectively. **(c)**, **(d)**, (**g** and **h**) differences for ARW and ORW latent heat fluxes, respectively.

HESSD
11, 5037–5075, 2014

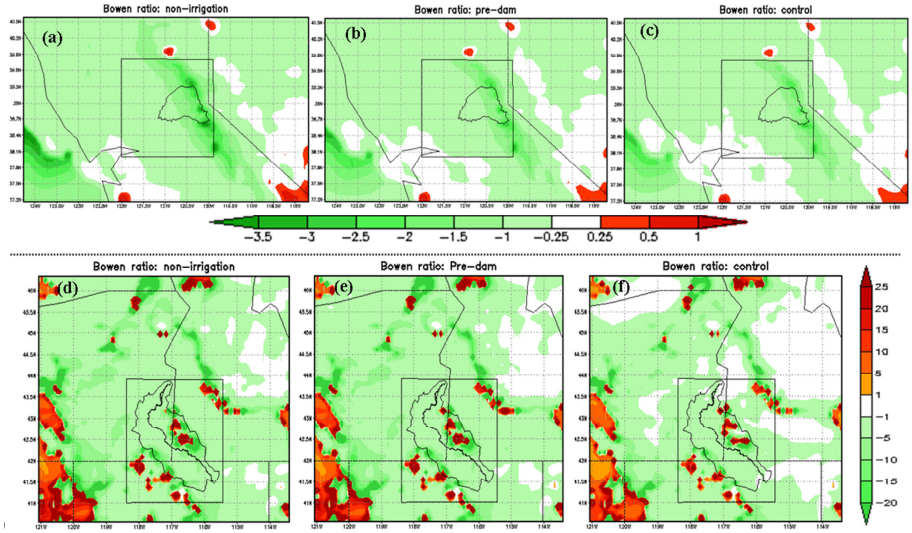

Fig. 7. Bowen ratios for ARW top panel and ORW bottom panel left to right represent *non-irrigation*, *pre-dam* and *control*.

HESSD
11, 5037–5075, 2014

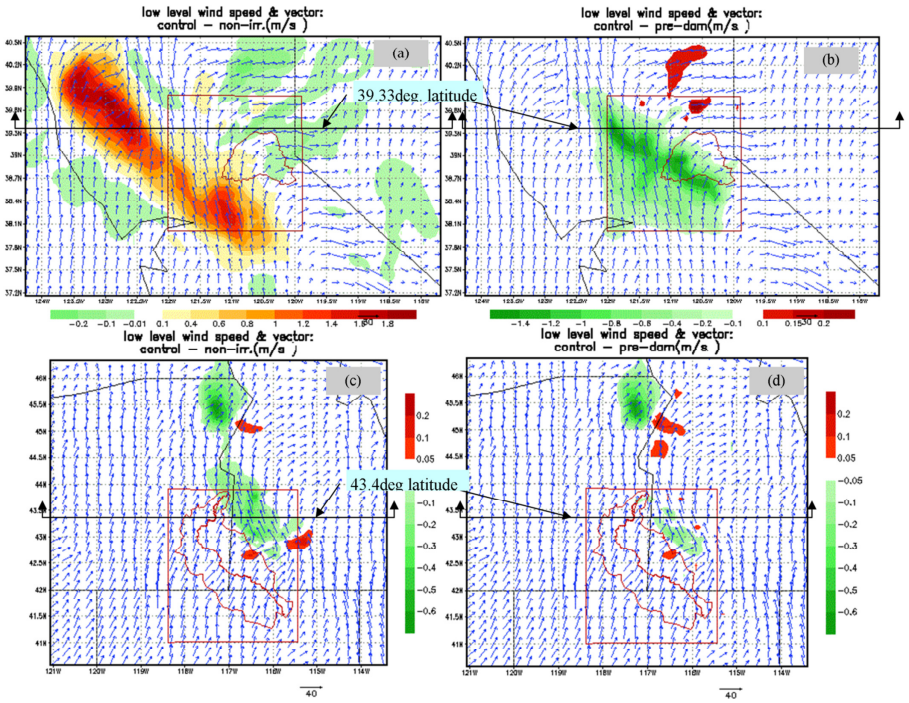

Fig. 8. low level wind speed ($m s^{-1}$) and vector. (**a** and **b**) for ARW, *control–non-irrigation* and *control–pre-dam* cases, respectively. (**c** and **d**) for ORW, *control–non-irrigation* and *control–pre-dam* cases, respectively.

HESSD
11, 5037–5075, 2014

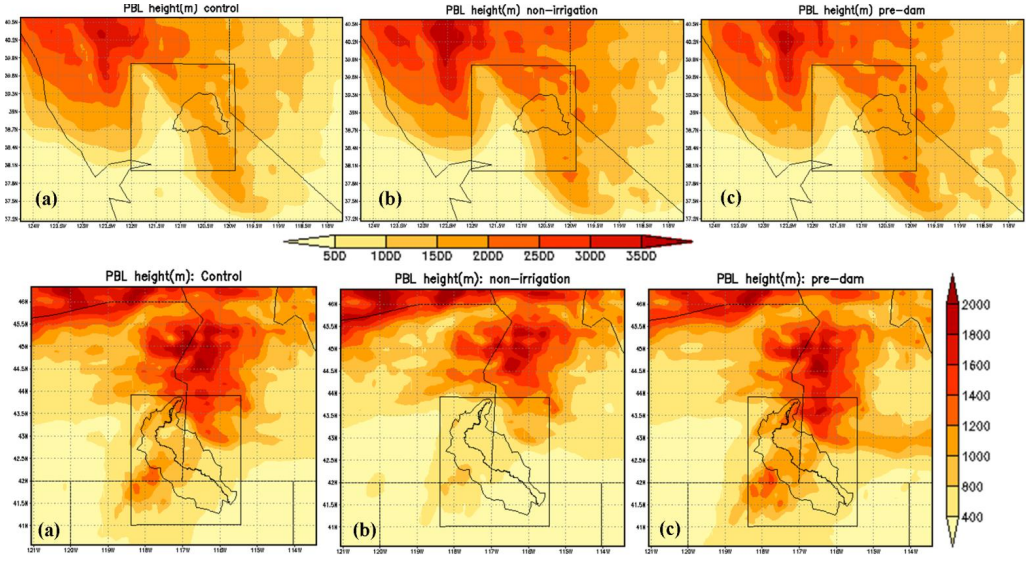

Fig. 9. The average depth of PBL (m) for each scenario and region. Top panel **(a)**, (**b** and **c**) represent *control, non-irrigation* and *pre-dam* for ARW while bottom panel **(a)**, (**b** and **c**) represent *control, non-irrigation* and *pre-dam* for ORW.

HESSD
11, 5037–5075, 2014

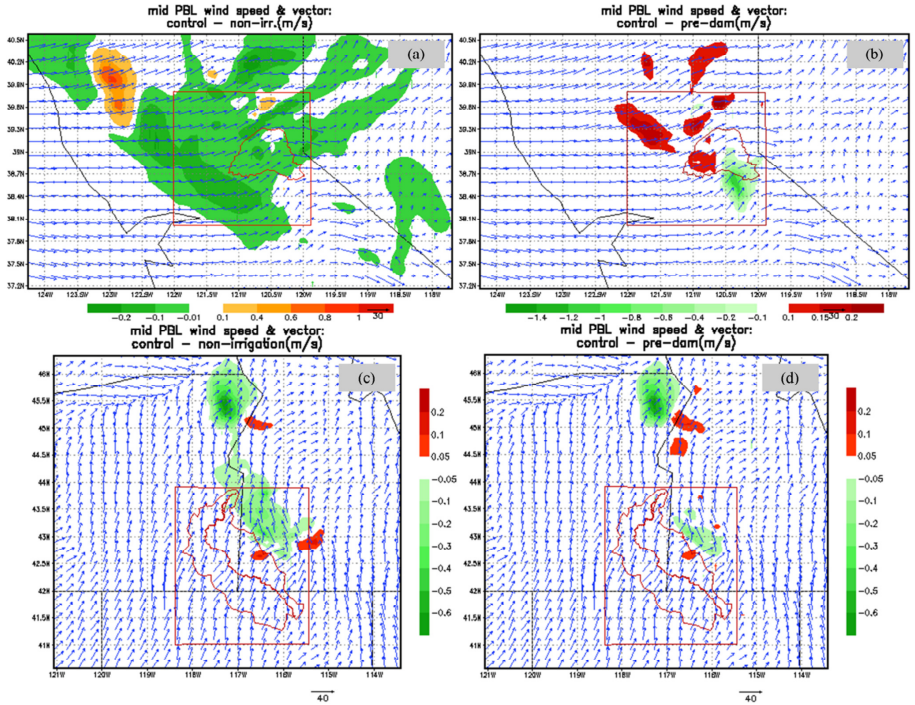

Fig. 10. Mid-PBL wind speed ($m\,s^{-1}$) and vector. (**a** and **b**) for ARW, *control–non-irrigation* and *control–pre-dam* cases, respectively. (**c** and **d**) for ORW, *control–non-irrigation* and *control–pre-dam* cases, respectively.

HESSD
11, 5037–5075, 2014

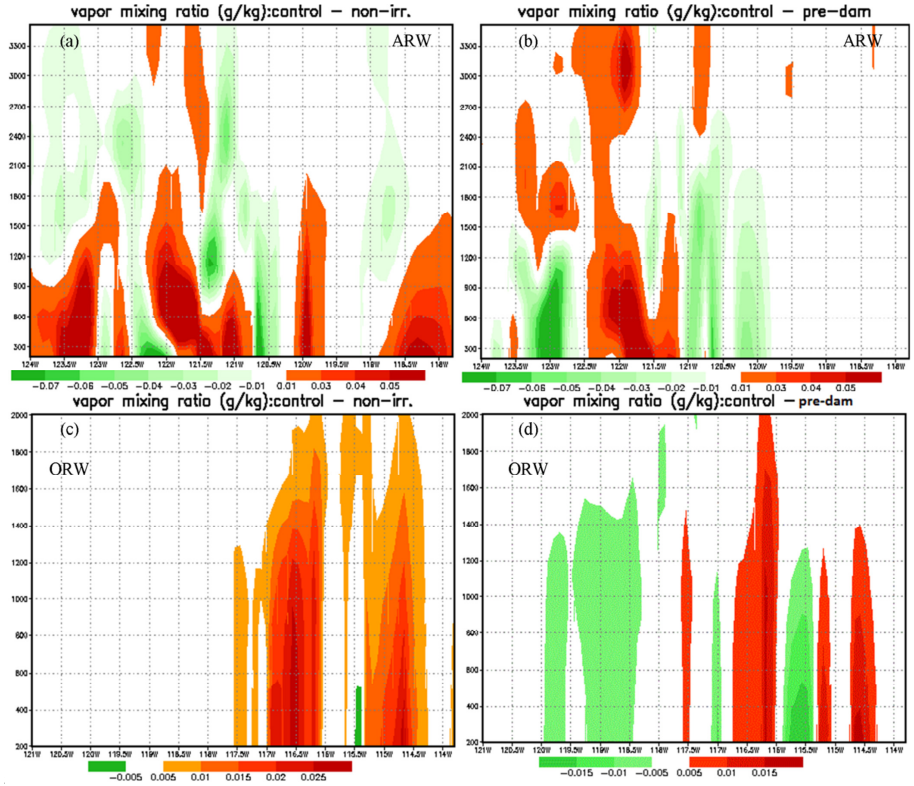

Fig. 11. Altitude-longitude cross-section of simulated vapor mixing ratio ($g\,kg^{-1}$). (**a** and **b**) for ARW (at 39.330° N) and (**c** and **d**) for ORW (at 43.40° N). All calculations are at 22:00 UTC (or 14:00 LST).

HESSD
11, 5037–5075, 2014

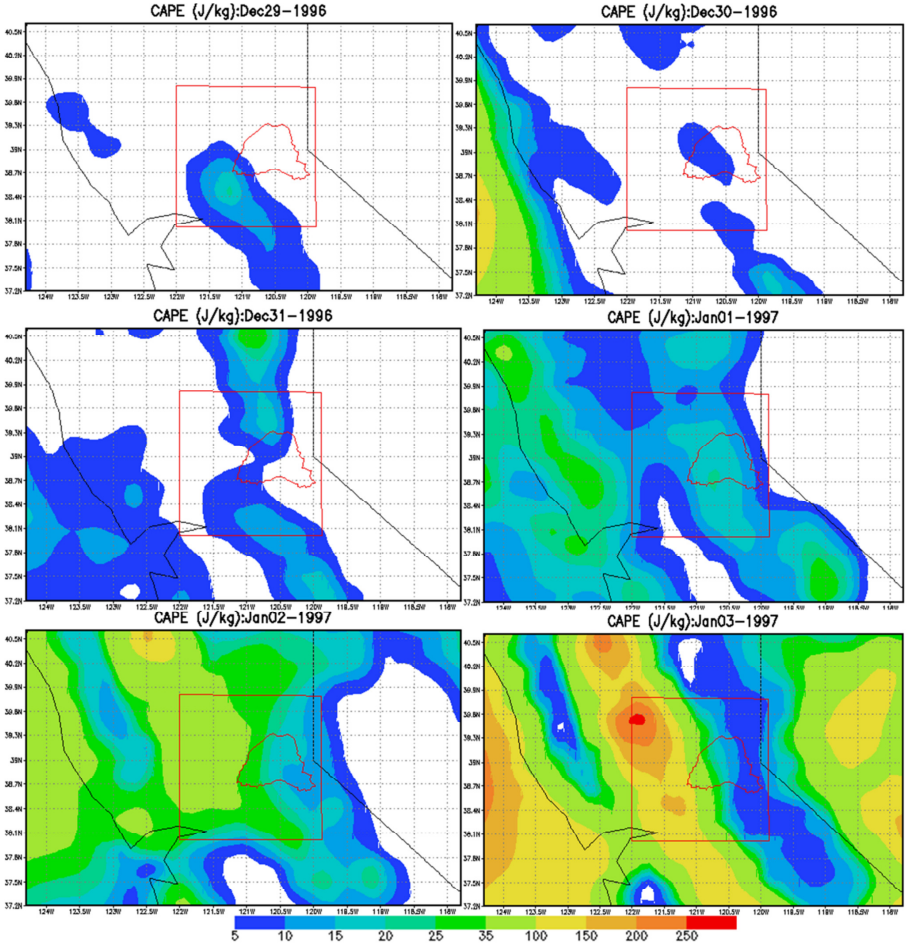

Fig. 12. Convective available potential energy (CAPE, $J kg^{-1}$) for considered six heavy storm days in ARW. The dates are shown at the top of each figure.

HESSD
11, 5037–5075, 2014

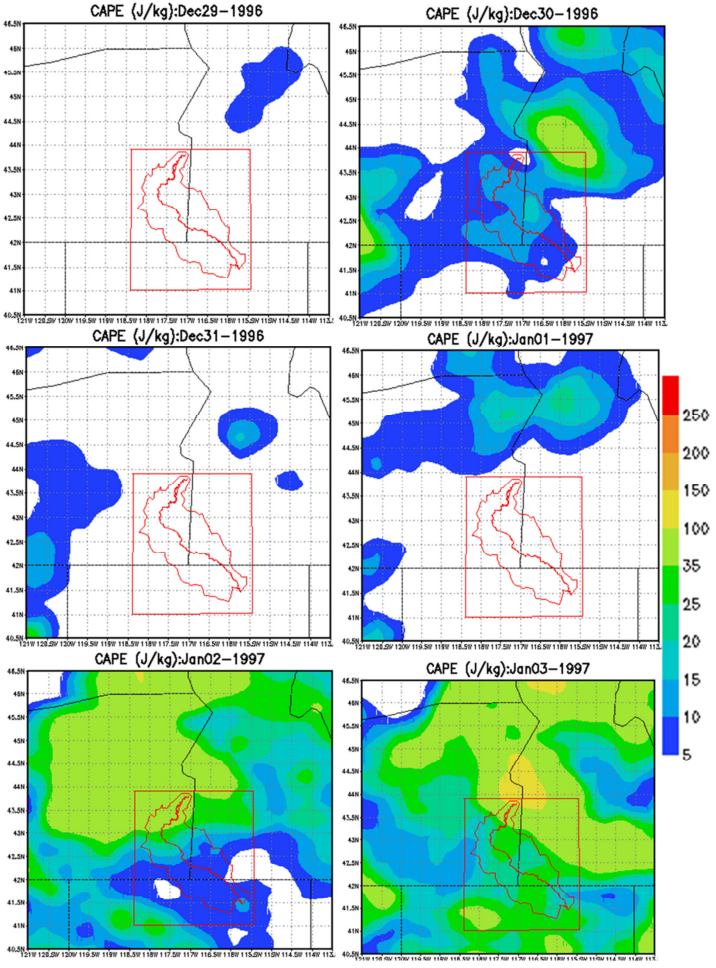

Fig. 13. Same as Fig. 12 but for ORW.

HESSD
11, 5037–5075, 2014